Elevated Temperature Thermal Properties of Carbon Steels used in Cold-Formed Light Gauge Steel Frame Systems

Edward Steau, Mahen Mahendran and Keerthan Poologanathan
Queensland University of Technology (QUT), Brisbane, Australia

Abstract: Fire design of cold-formed Light gauge Steel Frame (LSF) systems requires an accurate assessment of the thermal properties of each component at elevated temperatures. Heat transfer models based on these properties are implemented in order to accurately simulate the thermal behaviour of LSF systems in fire. For all carbon steel components, thermal properties are presented in Eurocode 3 Part 1.2. To verify the accuracy of thermal properties in Eurocode 3 Part 1.2 for the cold-formed steel components used in LSF construction, a series of thermal property tests was conducted based on the ASTM standard test methods. Thermal property tests were conducted to determine the specific heat at constant pressure, relative density, thermal conductivity and thermal diffusivity of three types of carbon steels, namely Grade 500 steel, Grade 300 steel and Grade 140 steel, due to their use in LSF construction. Test results showed the differences between the Eurocode 3 Part 1.2 model for carbon steels and the measured thermal property data for both specific heat and thermal conductivity of all three types of carbon steels due to chemical composition and the influence of carbon content. Hence, new equations were developed for specific heat and thermal conductivity for the selected carbon steels. To verify the effect of the measured thermal property results, 3-D heat transfer models of LSF floor-ceiling systems were developed and analysed. New thermal properties of carbon steels were used as inputs and comparisons made against fire test results for validation purposes. This paper presents the thermal properties of three selected carbon steels, which are commonly used in cold-formed LSF systems and the results.

Corresponding author's email address: m.mahendran@qut.edu.au

1.0 Introduction

Fire design of cold-formed Light gauge Steel Frame (LSF) systems requires good knowledge and understanding of the elevated temperature thermal properties of all the components used in their construction. These thermal properties are required to numerically model the thermal behaviour of LSF systems and to accurately predict their fire resistance characteristics. Hence, an accurate assessment of the basic elevated temperature thermal characteristics of the component materials is important. The thermal properties that are needed in the finite element heat transfer modelling include specific heat at constant pressure (C_p), relative density (ρ), thermal conductivity (λ) and thermal diffusivity (α) [1,2].

LSF systems are made of thin-walled cold-formed steel structural members as their framing elements such as their stud and joist sections and lined with gypsum plasterboards. In recent times, LSF systems are also constructed with thin steel sheathing to improve their thermal and structural performance [3-5]. These cold-formed LSF system components are constructed by using both low and high strength steels that are typically manufactured from coil carbon steel. For all carbon steels, thermal properties at elevated temperatures (20°C to 1200°C) are presented in Eurocode 3 Part 1.2 [6]. Figures 1 (a) and (b) show the specific heat and thermal conductivity of carbon steel as a function of temperature.

Craveiro et al. [7] conducted thermal property tests to determine the specific heat and thermal conductivity of S280GB+Z steel used in cold-formed steel construction (see Figures 2 (a) and (b)). They found that the Eurocode 3 Part 1.2 [6] model for thermal conductivity was unconservative for the type of steel tested. The difference was about 20% for the entire temperature range of 20°C to 800°C. They showed that this difference was due to the chemical composition of the type of carbon steel tested. Steels with higher levels of ferrite (Fe) and with lower levels of manganese (≈0.3%) (Mn) tend to have thermal conductivity values higher than 70 W/m°C [7]. Hence, it appears that Eurocode 3 Part 1.2 [6] should adopt different thermal conductivity models based on the chemical composition of steel. Peet et al. [8] predicted the thermal conductivities of various alloying elements within diluted solutions as shown in Figure 3. They showed that alloying elements do not have the equivalent effects in relation to thermal conductivity and instead are a function of the chemical composition of the steel type (see Figure 3).

This paper presents the details of the thermal property tests of three types of carbon steels (Grade 500 steel, Grade 300 steel and Grade 140 steel known as DX51D steel), which are used in cold-formed LSF systems. Grade 500 and 300 steels represent the high strength and low strength cold-formed steel grades in Australia and New Zealand whereas Grade 140 steel is used in commercial fire protective products, in particular as steel sheathing linings. Tests were conducted based on ASTM E1269 [9] and ASTM E1461 [10] standard test methods and the results are given as a function of temperature for specific heat at constant pressure, relative density, thermal conductivity and thermal diffusivity for each carbon steel. Thermal property tests were conducted on cold-rolled carbon steels which ranged from low to high strength steels (Grade 140 to 500) in order to establish reliable and improved understanding of their thermal characteristics.

2.0 Thermal Property Test Details and Standard Test Methods

In order to determine the thermal properties (specific heat at constant pressure (C_p), relative density (ρ), thermal conductivity (λ) and thermal diffusivity (α)) of carbon steels used in cold-formed LSF systems, a range of thermal analysis instruments is required. The changes in dimension and mass, phase transitions, enthalpies and rate of heat transfer as functions of the temperature of each carbon steel were investigated by simultaneous thermal analysis (STA) - NETZSCH STA 449 F3 Jupiter and laser flash analysis (LFA) - NETZSCH LFA 467 HyperFlash. Table 1 shows the thermal analysis instruments used in this study to measure the thermal properties of carbon steels. Table 2 gives the description of carbon steels with varying strength grade tested in this study. Table 3 shows their mechanical property requirements while their chemical composition requirements are given in Table 4.

2.1 Specific Heat at Constant Pressure and Relative Density

Specific heat at constant pressure (C_p) and relative density (ρ) measurements were obtained using simultaneous thermal analysis (STA). The principle of STA is shown in Figure 4 whereby differential scanning calorimetry (DSC) and thermogravimetric analysis (TGA) measurements are applied simultaneously to the same sample. Differential scanning calorimetry is a technique in which the heat flow rate to the sample is monitored. The difference in heat flow rate to the sample compared to a reference material (sapphire standard) is monitored. It measures endothermic and exothermic transitions as a function of temperature.

3

- Endothermic - heat flows into a sample
- Exothermic - heat flows out of a sample

Thermogravimetric analysis is a technique in which the mass of the sample is monitored as a function of temperature or time, while the sample is subjected to a controlled temperature program in a specified atmosphere. Hence simultaneous DSC-TGA measurements of both heat flow and weight change of a sample are obtained as a function of temperature or time under controlled atmosphere. Simultaneous measurements of these two material properties not only improve productivity but also simplify interpretation of the results. The complimentary information obtained allows differentiation between endothermic and exothermic events, which are not associated with weight change (i.e. melting and crystallisation) and those which involve a weight change (i.e. degradation). Equation 1 presents the standard equation given in ASTM E1269 [9] for specific heat calculation with heat flow calibration condition while Equation 2 considers the mass loss variation with temperature.

$$C_p(s) = C_p(st) \cdot \frac{D_s \cdot W_{st}}{D_{st} \cdot W_s} \qquad (1)$$

where

$C_p(s)$	=	specific heat capacity of the specimen, $J/(g * K)$
$C_p(st)$	=	specific heat capacity of sapphire standard, $J/(g * K)$
D_s	=	vertical displacement between the specimen holder and the specimen DSC thermal curves at a given temperature, mW
D_{st}	=	vertical displacement between the specimen holder and the sapphire DSC thermal curves at a given temperature, mW
W_s	=	mass of specimen, mg
W_{st}	=	mass of sapphire standard, mg

$$C_p(actual) = C_p(software) \cdot \frac{1}{mass\ loss} \qquad (2)$$

The instruments used were the NETZSCH STA 449 F3 Jupiter shown in Figure 5. It shows the two STA instruments used in this study. The instrument on the left (STA1) contains a rhodium furnace that can be heated to 1650°C while the instrument on the right (STA2) contains a platinum furnace that can be heated to 1500°C. The instruments were calibrated for temperature and sensitivity using a melting point method and the materials used for calibration were In, Sn, Zn, Al, Ag and Au. Heat flow calibration was performed prior to every specific heat

measurement using a sapphire disk and the procedures given in Step 2. Both instruments were used to obtain the specific heat at constant pressure and relative density measurements for all the carbon steels investigated.

Tests were conducted according to the standard procedures presented in ASTM E1269 [9] using Platinum (Pt) crucibles lined with Alumina (Al_2O_3) liners and Platinum (Pt) pin holed lids (see Figure 6). The crucibles were covered with a pin holed lid to simulate the environment developed by the heating of materials tested in the crucibles. Each test was conducted using a defined procedure presented in ASTM E1269 [9], which included:

Step 1: Baseline Measurement
When determining the baseline measurement, both reference and sample crucibles were empty. The reference and sample crucibles and lids were weighed and the masses were kept within 1% of each crucible. The baseline measurement was conducted in a purged environment using nitrogen gas inert atmosphere at a flow rate of 50 ml/min and with the sample temperature controller (STC) off. Nitrogen gas is an inert gas that does not affect the reactions in the samples considered. Three evacuations and refills of nitrogen gas preceded each measurement to ensure an absolute purged environment before the measurements. The temperature program for the measurements was set to start from 25°C and then increase to 1200°C at a rate of 20°C/min. This heating rate was used based on the procedure specified in the ASTM E1269 [9] for determining the specific heat capacity. A 15 minute isothermal segment was maintained at both 25°C and 1200°C. Platinum (Pt) crucibles lined with Alumina (Al_2O_3) liners and pin holed lids were used for all thermal property tests. Baselines were repeated when necessary until the baseline measurement were repeatable.

Step 2: Measurement of Sapphire Standard
Sapphire was selected as the standard material (reference material). The measurement of the sapphire standard was based on the previous baseline measurement. The reference crucible was empty while a sapphire disc was weighed and placed in the sample crucible. The difference in heat flow between the empty crucible and the reference material (sapphire) of known specific heat was recorded. Based on ASTM E1269 [9], sample material masses of about 5 to 15 mg for organic liquids and solids and 20 to 50 mg for inorganic specimens are recommended. Since all carbon steels are inorganic a 20 mg sapphire disc mass was selected. A 0.25 mm (20.6 mg and 20.9 mg) sapphire disc supplied by NETZSCH was used as the reference standard material

of known heat flow. Figures 7 shows the sapphire discs and the procedure of placement in the crucible.

Step 3: Measurement of Sample Material

The sample materials (carbon steel) were made into a powder form and each sample material was measured for the initial mass of 20 mg. The reference crucible was kept empty. The sample material was compressed to ensure a direct contact with the base of the crucible. The DSC measurement and the mass retention variations with temperature using TGA of the test materials were obtained simultaneously. The difference in heat flow between the empty and sample crucibles was also recorded. The specific heat was then calculated using a ratio between these two measurements (see Equations 1 and 2). Figure 8 shows the powdered grade 300 steel before and after the STA test.

2.2 Thermal Conductivity and Thermal Diffusivity

Thermal diffusivity at elevated temperatures was obtained using the laser flash analysis technique adopted in NETZSCH LFA 467 Hyperflash. The laser flash method first introduced by Parker et al. [11] is capable of conducting noncontact measurements of thermal diffusivity, heat capacity and thermal conductivity of various materials. Thermal diffusivity ((α) (mm^2/s)) is a measurement of thermal inertia of a material. This thermal property provides awareness of how fast heat is propagated through the medium. The flash method was primarily developed to measure thermal diffusivity. Figure 9 (a) shows the principle of how thermal diffusivity (α) is determined. The front side of the investigated material sample is heated up by a high intensity, short duration light (laser) pulse. The resulting change of temperature with time on the back side of the sample is recorded by an infrared camera. A typical curve of temperature rise versus time is shown in Figure 9 (b). A mathematical analysis of this graph allows the determination of the thermal diffusivity.

The NETZSCH LFA 467 Hyperflash allows the measurements of the thermal diffusivity at pre-programmed temperatures. In this study, a heating rate of 20°C/min in a purged environment using Nitrogen gas at a rate of 50 ml/min was used for all the carbon steel measurements. Thermal diffusivity data were obtained at every 20°C interval segments starting from 30°C and ending at 500°C. For each temperature condition three shots were executed for each test sample in order to obtain average thermal diffusivity results. The samples were placed

6

in a specialised sample holder for testing thin and highly conducting samples. Solid square samples of dimensions 10 mm x 10 mm were cut from each carbon steel material. The zinc coating was removed prior to testing in order to allow only the base metal to be tested. The sample materials were sprayed with three thin coats of graphite on each face of the sample. Liquid nitrogen was added to the NETZSCH LFA 467 Hyperflash during testing. Equation 3 gives the relationship between the parameters for determining thermal conductivity. The thermal conductivity variation with temperature was calculated using Equation 3, where the temperature dependent thermal conductivity, $\lambda(T)$ in W/m°C is defined as a function of thermal diffusivity (α(T) in mm^2/s), specific heat at constant pressure (C_p in J/kg°C), and relative density (ρ(T) in kg/m^3). Figure 9 (c) shows the NETZSCH LFA 467 Hyperflash used in this study to measure the thermal diffusivity of carbon steels.

$$\lambda(T) = a(T) \cdot C_p \cdot \rho(T) \qquad\qquad (3)$$

3.0 Thermal Property Test Results and Discussions

This section presents the thermal property results for the three types of cold-rolled carbon steels (Table 2) as a function of temperature. Relevant thermal property measurements were obtained by using NETZSCH STA 449 F3 Jupiter to determine the specific heat at constant pressure and the relative density and by using NETZSCH LFA 467 Hyperflash to determine the thermal conductivity and the thermal diffusivity. Multiple tests were conducted for each carbon steel sample material and test procedure in order to establish reliable results.

3.1 Specific Heat at Constant Pressure and Relative Density Measurements

Figures 10 to 13 show the measured thermal properties as a function of temperature for the three carbon steels. All the test samples exhibited similar specific heat versus temperature characteristics with two endothermic reactions in the temperature range of 36 to 1180°C. The average measured thermal properties are used in the discussions.

Figure 10 (a) shows the raw data from DSC and TGA measurements from the STA instrument while Figure 10 (b) shows the calculated C_p results evaluated with the C_p ratio method and sapphire standard for Grade 500 steel. Figures 11 (a) and (b) show the plots of specific heat and mass loss variations for Grade 500 steel. Figure 11 (a) shows that the first sudden

7

endothermic reaction occurred at 768°C for Grade 500 steel. At this temperature, the specific heat value measured was 1154 J/kg°C. A second sudden endothermic reaction occurred at 920°C and at this temperature, the specific heat value measured were 2043 J/kg°C. Figure 11 (b) shows no mass loss variation for Grade 500 steel for the completed temperature range of 36 to 1180°C.

Figures 12 (a) and (b) show the plots of specific heat and mass loss variations for Grade 300 steel. Figure 12 (a) shows that the first sudden endothermic reaction occurred at 744°C and then at 764°C for Grade 300 steel. At these temperatures, the specific heat values measured were 1143 J/kg°C and 1200 J/kg°C, respectively. During this phase transition, the specific heat gradually increased linearly to the highest value of 1200 J/kg°C rather than a single peak. A second sudden endothermic reaction occurred at 908°C and at this temperature, the specific heat value measured was 950 J/kg°C. Figure 12 (b) shows no mass loss variation in the completed temperature range of 36 to 1180°C for Grade 300 steel.

Figures 13 (a) and (b) show the plots of specific heat and mass loss variations for Grade 140 steel. The first sudden endothermic reactions occurred at 740°C and then at 766°C for Grade 140 steel. At these temperatures, the specific heat values measured were 1094 J/kg°C and 1210 J/kg°C, respectively. A second sudden endothermic reaction occurred at 918°C and at this temperature, the specific heat value measured was 2100 J/kg°C. Figure 13 (b) shows no mass loss variation for Grade 140 steel in the temperature range of 36 to 1180°C.

Figures 14 (a) and (b) show the comparisons of average specific heat and mass loss variations for the three grades of steel. Their specific heats at the initial temperature were 516, 475 and 551 J/kg°C. The specific heat increased slowly with temperature up to 600°C and then increased at a faster rate in the range of 600 to 700°C. A sudden endothermic reaction occurred at 768°C, 764°C and 766°C for Grade 500 steel, Grade 300 steel and Grade 140 steel, respectively. At these temperatures, the specific heat values measured were 1154, 1200 and 1210 J/kg°C. When steel is heated beyond 700°C, its microstructure undergoes the arrangement of atoms from a body centred cubic crystal structure to a face centred cubic crystal structure. This denotes the change in magnetic properties in steel of magnetic to nonmagnetic transformation (a second-order transition) and does not represent a phase change [15,16]. During the magnetic transformation, the steel absorbs thermal energy, resulting in the increase in specific heat. A second sudden endothermic reaction occurred at 920°C, 908°C and 918°C

8

for Grade 500 steel, Grade 300 steel and Grade 140 steel, respectively. At these temperatures, the specific heat values measured were 2043, 950 and 2100 J/kg°C. This denotes the phase transition from α-ferrite to γ-austenite [15,16], a first-order transition in carbon steel, which resulted in the significant increase in specific heat.

Figure 15 compares the measured carbon steel thermal property results from the tests with those from the models presented in Eurocode 3 Part 1.2 [6] and ASCE [17]. Both Eurocode 3 Part 1.2 [6] and ASCE [17] models show little variations in specific heat with test data below the temperature of 700°C. However, differences are apparent beyond 700°C. These differences are considered to be due to the differences in the chemical composition, in particular carbon content. The influence of carbon content results in changes to specific heat, which occur near the Curie point [18]. Figure 15 shows that the Eurocode 3 Part 1.2 [6] model is unsafe for the specific heat while the ASCE [17] model agrees reasonably well for the cold-formed steel components used within LSF construction. Therefore, new models are proposed in Section 4 to determine the specific heat values of cold-formed carbon steels. Figure 16 extends the comparisons to Craveiro et al. [7], Kodur et al. [18], Choi et al. [19] and Fang et al. [20], which show similar differences occurring after 700°C. It shows that the specific heat capacities of different types of steels heated beyond 700°C follow different trends because of varying chemical composition [18].

3.2 Thermal Conductivity and Thermal Diffusivity Measurements

Thermal diffusivity values were not measured after 500°C due to the limitations in the measuring equipment. Multiple tests were conducted in order to establish average reliable results for thermal diffusivity and thermal conductivity. From thermogravimetric analysis (TGA) in Section 3.1 (see Figures 11 (b) to 13 (b)), no mass loss variation occurred for all three types of carbon steels in the temperature range of 36 to 1180°C. Hence the density of steel was kept constant as 7850 kg/m^3 in this temperature range.

Figure 17 (a) shows the raw data from the single shots of the thermal diffusivity measurements from the LFA instrument for Grade 500 steel while Figure 17 (b) shows the measured temperature versus time curve at 300°C. Measurements considered cowan plus pulse correction model for diffusivity calculations in order to consider heat loss approximations and the short

duration time of the measurement. Figure 17 (b) shows a very short heat diffusion time for steel as the entire measurements last slightly over 150 milliseconds.

Figure 18 shows the measured thermal diffusivity values and thermal conductivity calculated using Equation 3 for Grade 500 steel. The thermal conductivity of Grade 500 steel reduces linearly from 30 to 500ºC and the values at these temperatures are 72.807 W/mºC and 34.615 W/mºC, respectively. Similarly, Figures 19 and 20 show the measured thermal diffusivity values and thermal conductivity calculated using Equation 3 for Grade 300 steel and Grade 140 steel, respectively. The thermal conductivity of Grade 300 steel reduces linearly from 30 to 500ºC and the values at these temperatures are 63.088 W/mºC and 30.981 W/mºC, respectively. The thermal conductivity of Grade 140 steel also varies linearly from 30 to 500ºC and the values at these temperatures are 82.575 W/mºC and 38.718 W/mºC, respectively.

Figure 21 compares the measured thermal conductivity results from the tests with those from the model presented in Eurocode 3 Part 1.2 [6] and ASCE [17] while Table 4 presents the requirements for chemical composition given within AS 1397 [12] for Grade 500 and Grade 300 steels and EN 10327 [13] for Grade 140 steel. Figure 21 shows the differences among the thermal conductivity values of these steels. Grade 140 steel exhibited the highest thermal conductivity value compared with others. They were 72.807 W/mºC and 34.615 W/mºC for Grade 500 steel, 63.088 W/mºC and 30.981 W/mºC for Grade 300 steel and 82.575 W/mºC and 38.718 W/m/ºC for Grade 140 steel at 30 and 500ºC. This difference is considered to be due to the difference in the chemical composition [7] with lower levels of Manganese (Mn) resulting in thermal conductivity values higher than 70 W/mºC. Grade 140 steel has lower levels of Manganese (Mn) (0.60%) for Grade 140 steel when compared with 1.20% and 1.60% for Grade 500 and Grade 300 steels, respectively, as shown in Table 4.

Table 4 also shows the differences in carbon content between Grade 500, 300 and 140 steels. Carbon content has significant influence on the thermal conductivity of steels, with higher carbon content leading to lower thermal conductivity values [18]. For the steels considered here, these carbon content values are 0.20%, 0.30% and 0.12% (Table 4) with corresponding thermal conductivity values at initial temperature of 72.807 W/mºC, 63.088 W/mºC and 82.575 W/mºC for Grade 500, 300 and 140 steel, respectively. Thermal conductivity of carbon steels decreases with increasing temperature and the initial differences at lower temperatures being based on chemical composition. However, with increasing temperature, this effect is known to

saturate and thermal conductivity becomes independent of temperature [8]. At higher temperatures where austenite forms (700 to 950ºC) all alloys have similar thermal conductivities [8]. Figure 21 shows that the Eurocode 3 Part 1.2 [6] and ASCE [17] thermal conductivity models for carbon steels are unsafe to use for the cold-formed steel components used in LSF construction. Therefore, new thermal conductivity models are proposed in Section 4.

4.0 Proposed Equations

This section proposes new models for both specific heat at constant pressure and thermal conductivity for Grade 500 steel, Grade 300 steel and Grade 140 steel based on the measured thermal property test results. New equations (Equations 4 to 32) are proposed to better represent the elevated temperature thermal characteristics of the three types of carbon steels used in LSF construction. Specific heat models are proposed for the temperature range of 20 to 1200°C while thermal conductivity models are proposed in three temperature ranges of 20 to 500ºC based on measured results, 500 to 950ºC and 950 to 1200ºC, resembling the model presented in Eurocode 3 Part 1.2 [6]. The proposed models of thermal conductivity account for the saturation of thermal conductivity in the region where austenite forms (phase transition of α-ferrite to γ-austenite). Hence, at 950ºC and after the completion of this phase transition, the thermal conductivity of all three carbon steels was kept the same as 27.3 W/m°C. Figures 22 to 24 show the proposed specific heat and thermal conductivity models for Grade 500 steel, Grade 300 steel and Grade 140 steel, respectively.

Grade 500 Steels

Specific heat at constant pressure (C_p) of Grade 500 steel:

For 20°C ≤ T < 600°C:

$$C_p = 521.62 + 1.144 \times 10^{-1}T + 3.0 \times 10^{-4}T^2 + 3.0 \times 10^{-7}T^3 \; J/kg°C \tag{4}$$

For 600°C ≤ T < 768°C: $C_p = 679 + \dfrac{17100}{804-T} \; J/kg°C$ (5)

For 768°C ≤ T < 900°C: $C_p = 694 + \dfrac{5985}{T-755} \; J/kg°C$ (6)

For 900°C ≤ T < 920°C: $C_p = 670 + \dfrac{1373}{921-T} \; J/kg°C$ (7)

For 920°C ≤ T < 1000°C: $C_p = 626 + \dfrac{1417}{T-919} \; J/kg°C$ (8)

For 1000°C ≤ T ≤ 1200°C: $C_p = 643 \; J/kg°C$ (9)

where: T is the steel temperature (°C)

Thermal conductivity (λ) of Grade 500 steel:

For 20°C ≤ T < 500°C: $\lambda = 73.181 - 8.07 \times 10^{-2}T \; W/m°C$ (10)

For 500°C ≤ T < 950°C: $\lambda = 38.977 - 1.23 \times 10^{-2}T \; W/m°C$ (11)

For 950°C ≤ T ≤ 1200°C: $\lambda = 27.3 \; W/m°C$ (12)

Grade 300 Steels

Specific heat at constant pressure (C_p) of Grade 300 steel:

For 20°C ≤ T < 600°C:

$$C_p = 495.88 - 1.294 \times 10^{-1}T + 8.0 \times 10^{-4}T^2 - 3.0 \times 10^{-7}T^3 \; J/kg°C \tag{13}$$

For 600°C ≤ T < 744°C: $C_p = 512 + \dfrac{23330}{781-T} \; J/kg°C$ (14)

For 744°C ≤ T < 764°C: $C_p = -977.4 + 2.85T \; J/kg°C$ (15)

For 764°C ≤ T < 900°C: $C_p = 662 + \dfrac{3765}{T-757} \; J/kg°C$ (16)

For 900°C ≤ T < 908°C: $C_p = -28787 + 32.75T \; J/kg°C$ (17)

For 908°C ≤ T < 1000°C: $C_p = 460 + \dfrac{980}{T-906} \; J/kg°C$ (18)

For 1000°C ≤ T ≤ 1200°C: $C_p = 470\ J/kg°C$ (19)

Thermal conductivity (λ) of Grade 300 steel:

For 20°C ≤ T < 500°C: $\lambda = 63.667 - 6.78 \times 10^{-2}T\ W/m°C$ (20)

For 500°C ≤ T < 950°C: $\lambda = 32.508 - 5.50 \times 10^{-3}T\ W/m°C$ (21)

For 950°C ≤ T ≤ 1200°C: $\lambda = 27.3\ W/m°C$ (22)

Grade 140 Steels

Specific heat at constant pressure (C_p) of Grade 140 steel:

For 20°C ≤ T < 600°C:

$$C_p = 544.45 - 9.55 \times 10^{-2}T + 1.0 \times 10^{-3}T^2 - 2.0 \times 10^{-7}T^3\ J/kg°C$$ (23)

For 600°C ≤ T < 740°C: $C_p = 702 + \frac{19200}{789-T}\ J/kg°C$ (24)

For 740°C ≤ T < 766°C: $C_p = 1063 + \frac{880}{772-T}\ J/kg°C$ (25)

For 766°C ≤ T < 906°C: $C_p = 663 + \frac{11480}{T-745}\ J/kg°C$ (26)

For 906°C ≤ T < 918°C: $C_p = 620 + \frac{1480}{919-T}\ J/kg°C$ (27)

For 918°C ≤ T < 1000°C: $C_p = 570 + \frac{3060}{T-916}\ J/kg°C$ (28)

For 1000°C ≤ T ≤ 1200°C: $C_p = 606\ J/kg°C$ (29)

Thermal conductivity (λ) of Grade 140 steel:

For 20°C ≤ T < 500°C: $\lambda = 82.922 - 9.23 \times 10^{-2}T\ W/m°C$ (30)

For 500°C ≤ T < 950°C: $\lambda = 47.296 - 2.10 \times 10^{-2}T\ W/m°C$ (31)

For 950°C ≤ T ≤ 1200°C: $\lambda = 27.3\ W/m°C$ (32)

5.0 Numerical Studies

In order to improve the accuracy and reliability of the fire design of LSF systems, finite element heat transfer modelling can be used and is used to determine the time-temperature curves for a given LSF system. In this section 3-D finite element heat transfer models of LSF floor-ceiling

systems were developed with inputs of the thermal properties of carbon steels proposed in Section 4. Finite element models were developed using heat transfer solid elements (DC3D8) with solid-solid tie constraints. Three modes of heat transfer; conduction, convection and radiation, were included. Conduction effects were based on the measured thermal properties. Convection effects were based on convective film coefficients assigned to the fire and ambient sides and were 25 and 10 $W/m^2/°C$, respectively. Radiation effects were assigned with the emissivity value of 0.9 for gypsum plasterboard while the Stefan-Boltzmann constant was defined as (σ) of $5.67x10^{-8}$ $W/m^2/°C^4$. Further details of the modelling techniques such as thermal boundary conditions, element type, constraints and convective film coefficients are given in Steau et al. [21].

Finite element heat transfer modelling was performed on an LSF floor system made of three 200x40x15x1.15 mm LCB joists with yield strength (f_y) = 500 MPa. The joists were spaced at 450 mm centres and were protected with two layers of 16 mm commercially available fire rated gypsum plasterboard on the fire exposed side and 19 mm F11 Stress Grade structural plywood on the unexposed side. Figure 25 shows the finite element model and allocated thermal boundary conditions of LSF floor-ceiling systems made of lipped channel section (LCS) joists. Experimental fire curve was assigned to the ceiling surface based on the ISO 834 standard fire curve [22]. Figure 26 shows the temperature contours across the LSF floor-ceiling systems made of LCS joists while Figure 27 compares the time-temperature profiles from the thermal finite element analyses with available fire test results [23]. Figure 27 (a) shows the time-temperature profiles at different interfaces across the floor depth while Figure 27 (b) shows them across the LCS joists in which the time-temperature profiles are identified with: FS – fire side (furnace temperature); PB-PB – plasterboard to plasterboard surface; PB-CAV – plasterboard to cavity surface; CAV-PLY – cavity to plywood surface; AS – ambient side; HF – hot flange of the joist; CF – cold flange of the joist.

Comparisons show a very good agreement between the developed 3-D finite element heat transfer models and fire test results for LSF floor-ceiling systems made of G500 LCS joists. Hence it is concluded that the new proposed models for specific heat at constant pressure and thermal conductivity based on thermal property measurements are able to predict the elevated temperature thermal characteristics of carbon steels.

Figures 28 (a) and (b) compare the time-temperature profiles at the different interfaces across the floor depth and the critical hot and cold flanges (HF and CF) obtained by using the developed thermal property models for specific heat and thermal conductivity and the models presented in Eurocode 3 Part 1.2 [6]. Despite the differences between the two thermal property models, the time-temperature profiles do not vary significantly across the LSF floor system. Since the cold-formed steel LCS joists are very thin (1.15 mm), the influence of specific heat and thermal conductivity on heat transfer was found to be negligible [24]. The differences in the critical hot flange temperatures were about 10ºC at 70 min with Eurocode 3 Part 1.2 [6] thermal property inputs predicting slightly higher time-temperature profiles when compared with the proposed model inputs.

6.0 Conclusions

This paper has presented the details and results of the thermal property tests of three cold-rolled carbon steels (Grade 500, 300 and 140 steels) that are used in the construction of LSF systems. Thermal property tests were conducted based on ASTM standard test methods and the results are given as a function of temperature for specific heat at constant pressure, relative density, thermal conductivity and thermal diffusivity for each carbon steel. Comparisons were made against the models presented in Eurocode 3 Part 1.2 [6] and ASCE [17] for specific heat and thermal conductivity. The specific heat models showed minor variations with test results below 700°C. However, beyond 700°C and within the region where steel undergoes the phase transition from α-ferrite to γ-austenite, significant differences were seen due to the variations in chemical composition and the influence of carbon content on the specific heat of carbon steels. Likewise, carbon content has a significant influence on the thermal conductivity of steels, with higher carbon content leading to lower thermal conductivity values. Although these differences occur at lower temperatures below 700°C, the effect saturates and all alloys have similar thermal conductivities with increasing temperature. Hence, new equations were proposed for specific heat at constant pressure and thermal conductivity of the three cold-rolled carbon steels based on the thermal property measurements reported in this paper.

Three-D heat transfer models of LSF floor-ceiling systems made of lipped channel section joists were developed with thermal properties based on both the proposed equations and the Eurocode 3 Part 1.2 model [6]. Heat transfer analyses showed that the differences in the time-

temperature profiles were small because of the thin cold-formed steel joists and their inability to significantly affect the heat transfer through the LSF floor-ceiling systems.

Acknowledgments

References

[1] Keerthan, P. and Mahendran, M. 2012a. Numerical studies of gypsum plasterboard panels under standard fire conditions. Fire Safety Journal. Vol. 53: pp. 105-119.

[2] Keerthan, P. and Mahendran, M. 2012b. Numerical modelling of non-load-bearing light gauge cold-formed steel frame walls under fire conditions. Journal of Fire Sciences. Vol. 30: pp. 375-403.

[3] Promat. 2012. Promat DURASTEEL High Performance Barriers and Ceiling Systems, Accessed May 23, 2018. http://www.promat-durasteel.co.uk/en/products/durasteel-panels.

[4] Yu, C. and Li, C. 2012. Behaviour and Strength of Cold-formed Steel Framed Shear Walls Sheathed with Composite Panels. Twenty-First International Specialty Conference on Cold-Formed Steel Structures. 24 - 25 October, 2012 St. Louis, Missouri, USA.

[5] Mohebbi, S., Mirghaderi, S. R., Farahbod, F., Sabbagh, A. B. and Torabian, S. 2016. Experiments on seismic behaviour of steel sheathed cold-formed steel shear walls cladded by gypsum and fibre cement boards. Thin-Walled Structures. Vol. 104: pp. 238-247.

[6] European Committee for Standardization (ECS). 2005. Eurocode 3: Design of Steel Structures - Part 1.2: General Rules - Structural Fire Design. EN 1993-1-2:2005. Brussels, Belgium.

[7] Craveiro, H. D., Rodrigues, J. P. C., Santiago, A. and Laím, L. 2016. Review of the high temperature mechanical and thermal properties of the steels used in cold formed steel structures - The case of the S280 Gd + Z steel. Thin-Walled Structures. Vol. 98: pp. 154-168.

[8] Peet, M. J., Hasan, H. S. and Bhadeshia, H. K. D. H. 2011. Prediction of thermal conductivity of steel, International Journal of Heat and Mass Transfer. Vol. 54: pp. 2602-2608.

[9]   ASTM E1269. 2018. Standard Test Method for Determining Specific Heat Capacity by Differential Scanning Calorimetry. ASTM International. West Conshohocken, PA, USA.

[10]   ASTM E1461. 2013. Standard Test Method for Thermal Diffusivity by the Flash Method. ASTM International. West Conshohocken, PA, USA.

[11]   Parker, W. J., Jenkins, R.J., Butler, C.P. and Abbott, G.L. 1961, Flash method of determining thermal diffusivity, heat capacity, and thermal conductivity, Journal of Applied Physics. Vol. 32, pp. 1679-1684.

[12]   Standards Australia (SA). 2011. Australia Standard Continuous hot-dip metallic coated steel sheet and strip-Coatings of zinc and zinc alloyed with aluminium and magnesium. AS 1397:2011. Sydney, Australia.

[13]   European Committee for Standardization (ECS). 2004. Continuously hot-dip coated strip and sheet of low carbon steels for cold forming - Technical delivery conditions. EN 10327:2004. Brussels, Belgium.

[14]   European Committee for Standardization (ECS). 2006. Eurocode 3: Design of Steel Structures - Part 1.3: General Rules – Supplementary rules for cold-formed members and sheeting. EN 1993-1-3:2006. Brussels, Belgium.

[15]   Kargul, T., Falkus, J. and Wielgosz, E. 2015. Application of Thermal Analysis Tests Results in the Numerical Simulations of Continuous Casting Process. Archives of Metallurgy and Materials. Vol.60: pp. 221-225.

[16]   Dossett, J. L. and Boyer, H. E. 2006. Practical Heat Treating. 2nd ed. Ohio: ASM International.

[17]   American Society of Civil Engineers (ASCE). 1992. Structural fire protection. ASCE 978-0-87262-888-5, ASCE Committee on Fire Protection, Structural Division, New York.

[18] Kodur, V., Kand, S. and Khaliq, W. 2012. Effect of Temperature on Thermal and Mechanical Properties of Steel Bolts. Journal of Materials in Civil Engineering. Vol. 24: pp. 765-774.

[19] Choi, I. R., Chung, K. S. and Kim, D. H. 2014. Thermal and mechanical properties of high-strength structural steel HSA800 at elevated temperatures. Materials and Design. Vol. 63: pp. 544-551.

[20] Fang, H., Wong, M. B. and Bai, Yu. 2017. Heating rate effect on the thermophysical properties of steel in fire. Journal of Constructional Steel Research. Vol.128: pp. 611-617.

[21] Steau, E., Keerthan, P. and Mahendran, M. 2017. Thermal Modelling of LSF Floor Systems made of Lipped Channel and Hollow Flange Channel Section Joists. 8th European Conference on Steel and Composite Structures. Copenhagen, Denmark. pp. 2638-2647.

[22] ISO 834. 2014. Fire Resistance Tests – Elements of Building Construction. International Organisation for Standardisation. Switzerland.

[23] Steau, E. 2019. Development of Fire Resistant Cold-Formed Steel Floor Systems. PhD Thesis. Queensland University of Technology. Brisbane, Australia.

[24] Hamerlinck, A. F. 1991. The Behaviour of Fire-Exposed Composite Steel/Concrete Slabs. PhD Thesis. Technische Universiteit Eindhoven. Eindhoven.

Table 1: Thermal Analysis Instruments

Instrument Name	Thermal Analysis	Thermal Property	Instrument
NETZSCH STA 449 F3 *Jupiter*	Differential Scanning Calorimetry (DSC)	Specific Heat at Constant Pressure (C_p)	
	Thermogravimetric Analysis (TGA)	Relative Density (ρ) / Mass Loss	
NETZSCH LFA 467 *HyperFlash*	Laser Flash Analysis (LFA)	Thermal Conductivity (λ)	
		Thermal Diffusivity (α)	

Table 2: Description of Materials Tested

Type of Material	Name of Material	Thickness of steel (mm)	Property Tested
Carbon Steel	Grade 500 Steel	1.15	C_p, λ, ρ and α
Carbon Steel	Grade 300 Steel	1.20	C_p, λ, ρ and α
Carbon Steel	DX51D Steel	0.50	C_p, λ, ρ and α

Note: Specific heat at constant pressure (C_p), thermal conductivity (λ), relative density (ρ) and thermal diffusivity (α)

Table 3: Mechanical Property Requirements for Structural Grades

Steel Grade Designation	Longitudinal Tensile Test		
	Min. Yield Strength (MPa)	Min. Tensile Strength (MPa)	Min. Elongation, % $L_0 = 80$ mm
*G500	500	520	7
*G300	300	340	18
**DX51D	140	270	22

Note: *   Requirements for mechanical properties as given in AS 1397 [12]

    **   Requirements for mechanical properties as given in EN 10327 [13] and EN 3 Part 1.3 [14]

Table 4: Requirements for Chemical Composition

Steel Grade Designation	Chemical Composition (cast analysis), % max.			
	Carbon (C)	Manganese (Mn)	Phosphorus (P)	Sulfur (S)
*G500	0.20	1.20	0.040	0.030
*G300	0.30	1.60	0.100	0.035
**DX51D	0.12	0.60	0.100	0.045

Note: *   Requirements for chemical composition as given in AS 1397 [12]

  **   Requirements for chemical composition as given in EN 10327 [13]
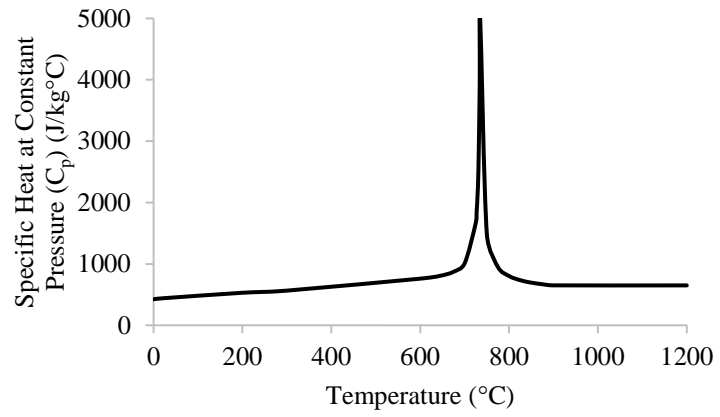
(a) Specific Heat at Constant Pressure
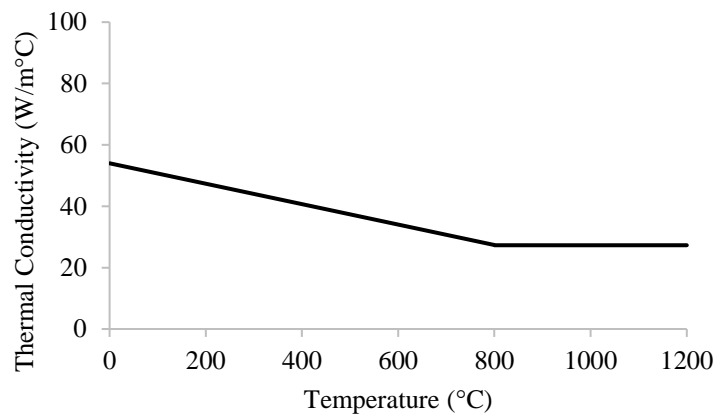
(b) Thermal Conductivity

Figure 1: Thermal Properties of Carbon Steel [6]
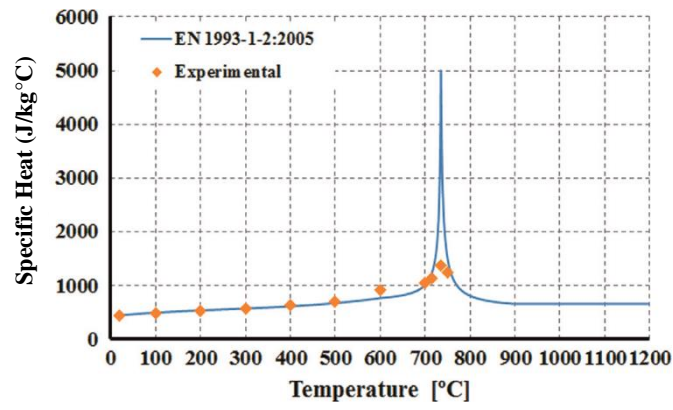
(a) Specific Heat at Constant Pressure
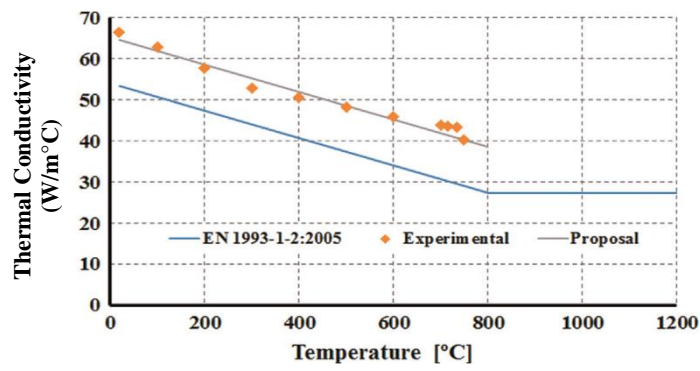
(b) Thermal Conductivity

Figure 2: Thermal Properties of S280GB+Z Steel [7]
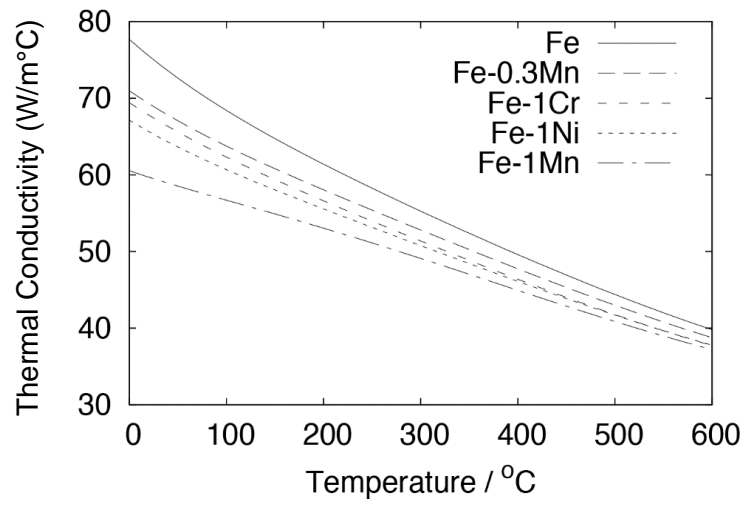
Figure 3: Prediction of the Thermal Conductivity of Dilute Solutions [8]

Figure 4: Differential Scanning Calorimetry (DSC) and Thermogravimetric Analysis (TGA)

(a) NETZSCH STA 449 F3 Jupiter
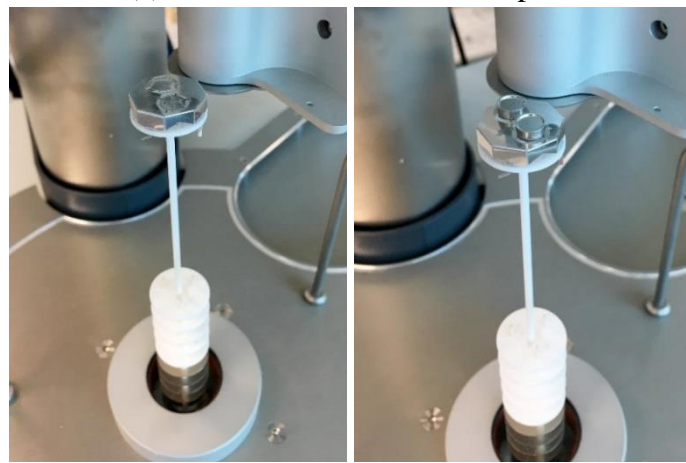
(b) STA1 sample holder with and without crucibles
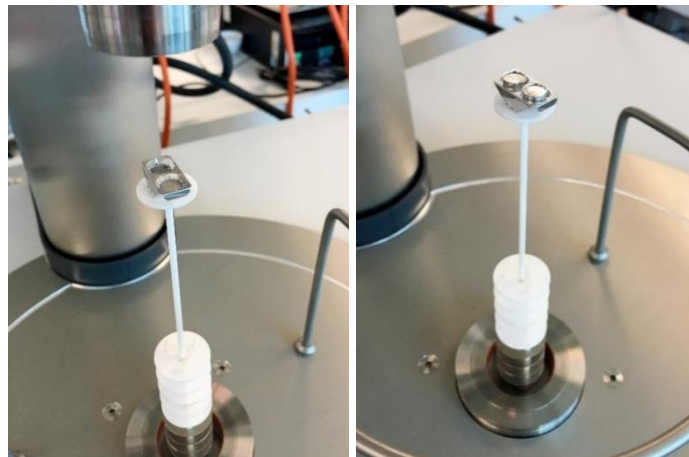
(c) STA2 sample holder with and without crucibles

Figure 5: NETZSCH STA 449 F3 Jupiter Instrument and Sample Holders

Figure 6: Platinum Crucibles Lined with Alumina Liners and Pin Holed Lids

(a) Different sizes of sapphire discs supplied by NETZSCH

(b) 0.25 mm (20.6 mg and 20.9 mg) sapphire disc placed in the crucible

Figure 7: Sapphire Disc (Reference Material)

(a) Before testing

(b) After testing

Figure 8: Powdered Grade 300 Steel Sample Before and After Test
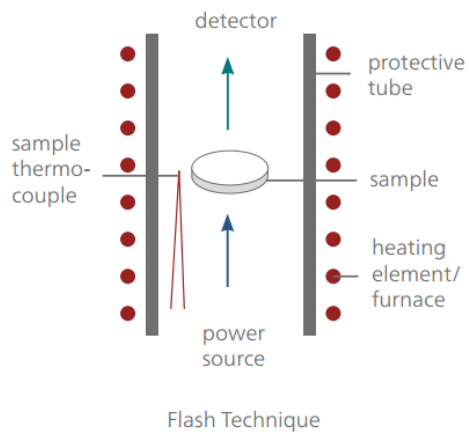
(a) Principle of the laser flash method
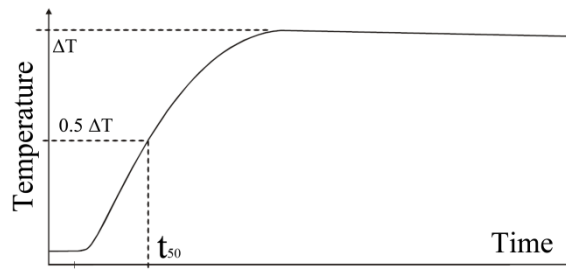
(b) Typical curve of temperature versus time
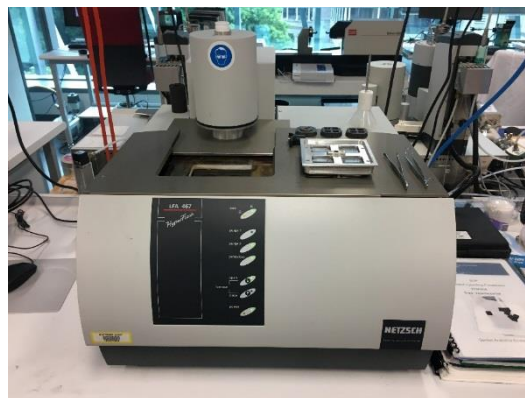
(c) NETZSCH LFA 467 Hyperflash Instrument

Figure 9: Laser Flash Method
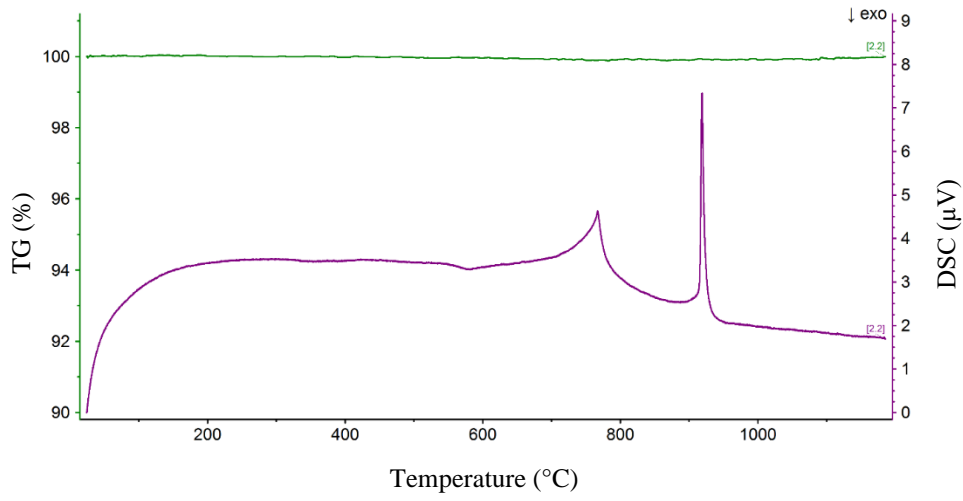
(a) DSC and TGA Measurements
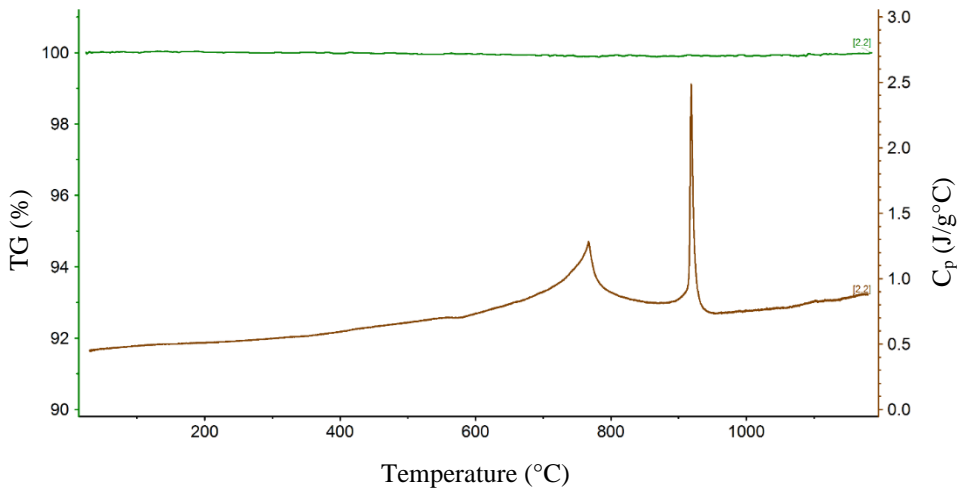
(b) C_p calculation

Figure 10: STA Measurements for Grade 500 Steel
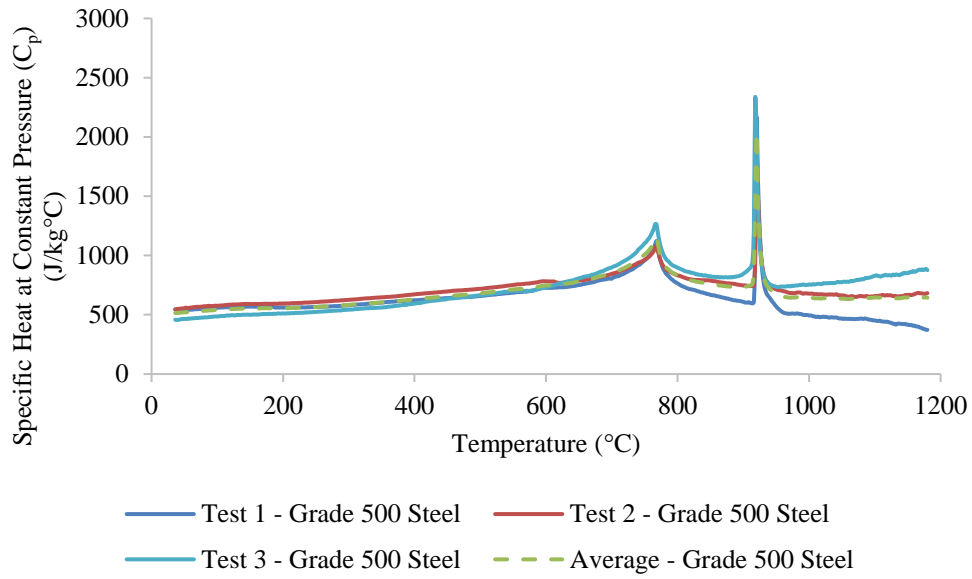
(a) Specific Heat at Constant Pressure
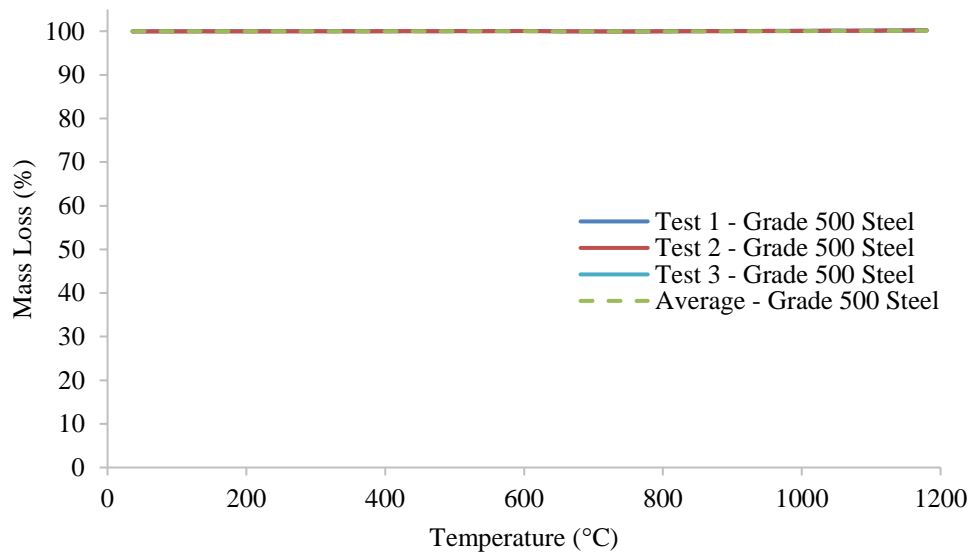
(b) Mass Loss

Figure 11: Plots of Specific Heat and Mass Loss Variations for Grade 500 Steel
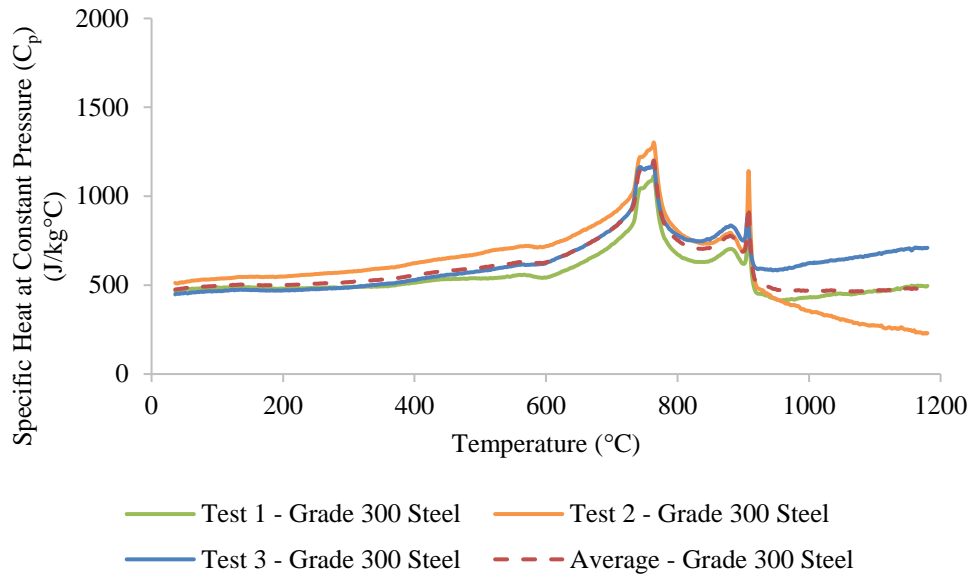
(a) Specific Heat at Constant Pressure
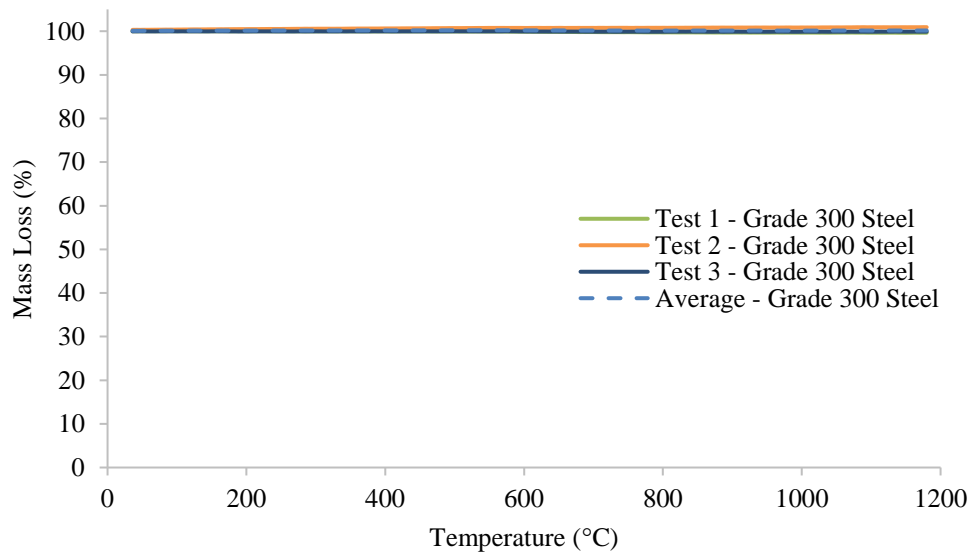
(b) Mass Loss

Figure 12: Plots of Specific Heat and Mass Loss Variations for Grade 300 Steel
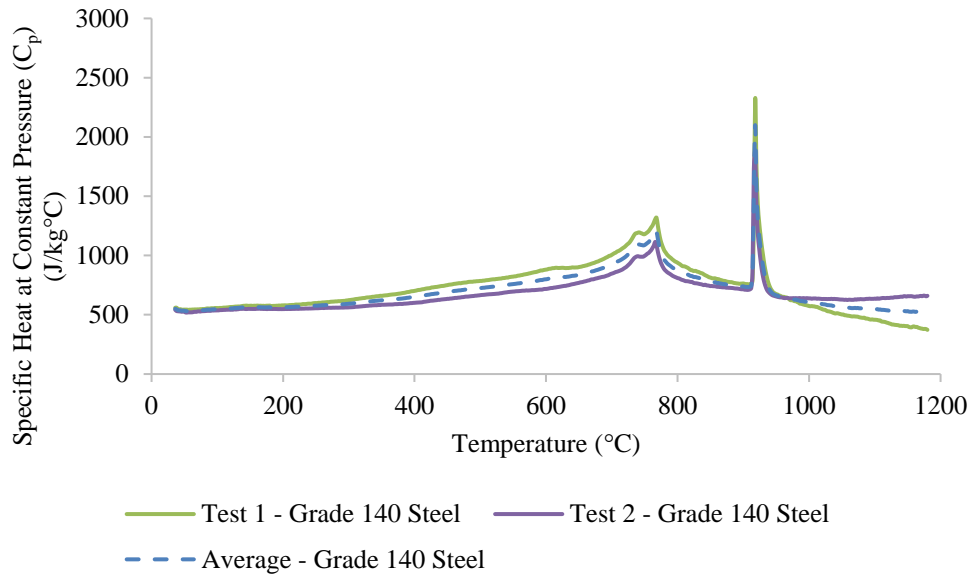
(a) Specific Heat at Constant Pressure
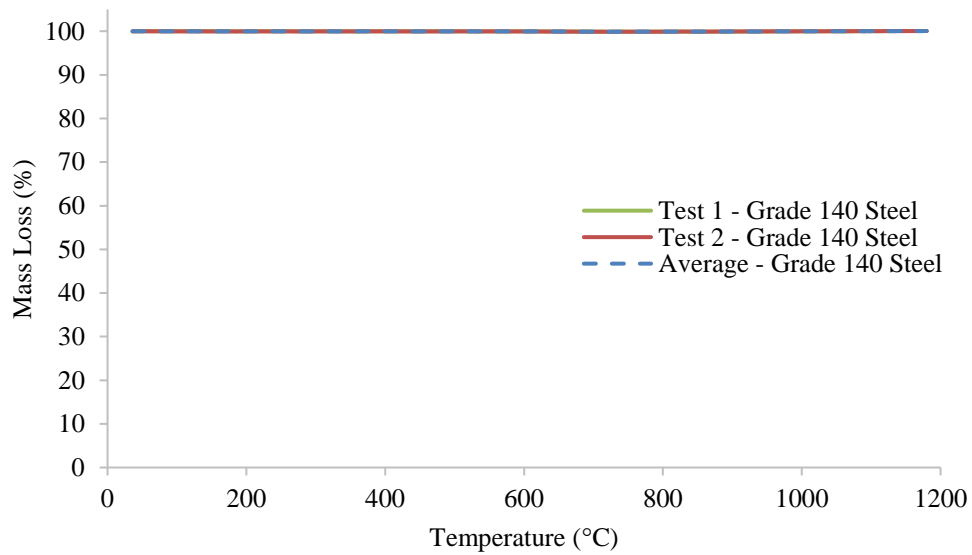
(b) Mass Loss

Figure 13: Plots of Specific Heat and Mass Loss Variations for Grade 140 Steel
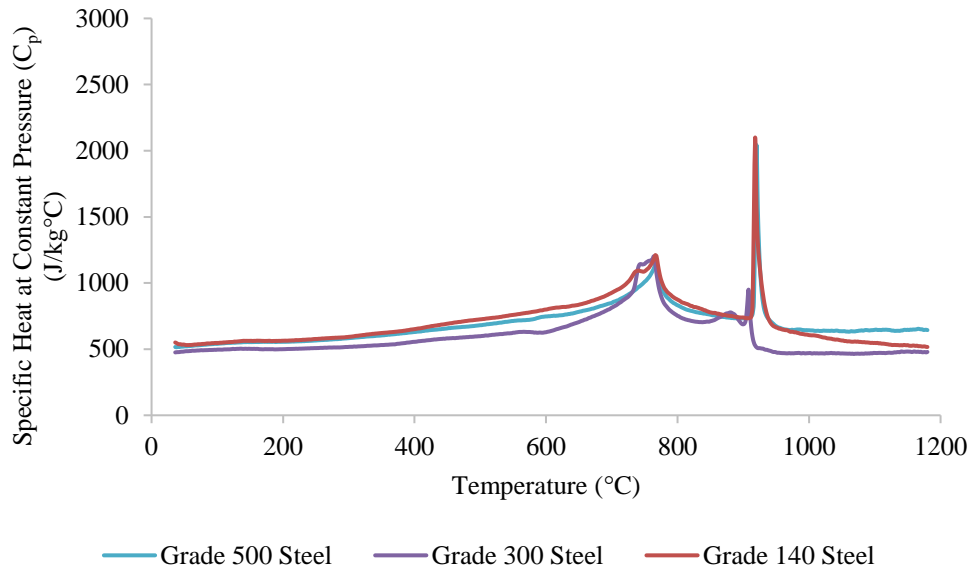
(a) Specific Heat at Constant Pressure
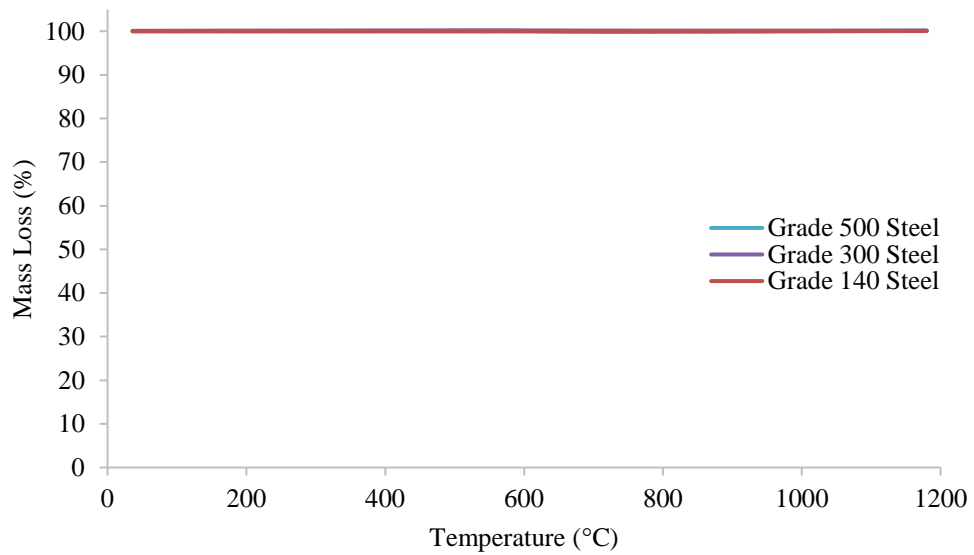
(b) Mass Loss

Figure 14: Comparisons of Specific Heat and Mass Loss Plots
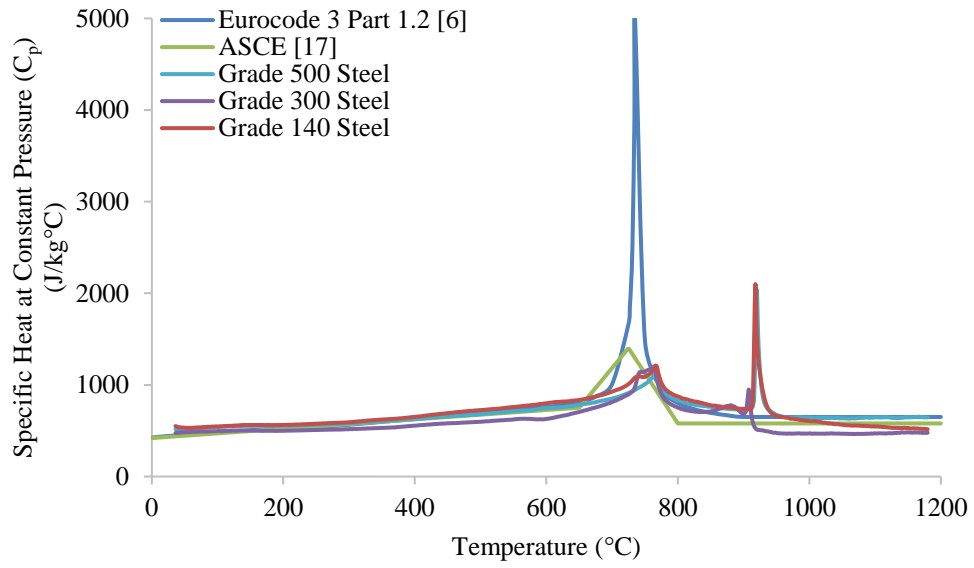
Figure 15: Comparison of Specific Heat Values of Cold-Formed Carbon Steels with Eurocode 3 Part 1.2 and ASCE Models
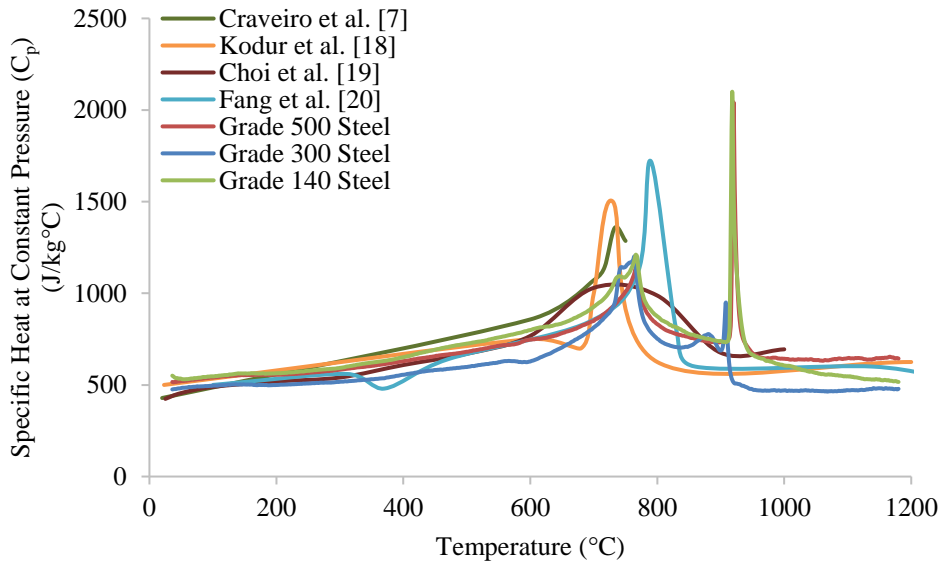
**Figure 16: Comparison of Specific Heat Values of Steels with other Researchers'
Results**
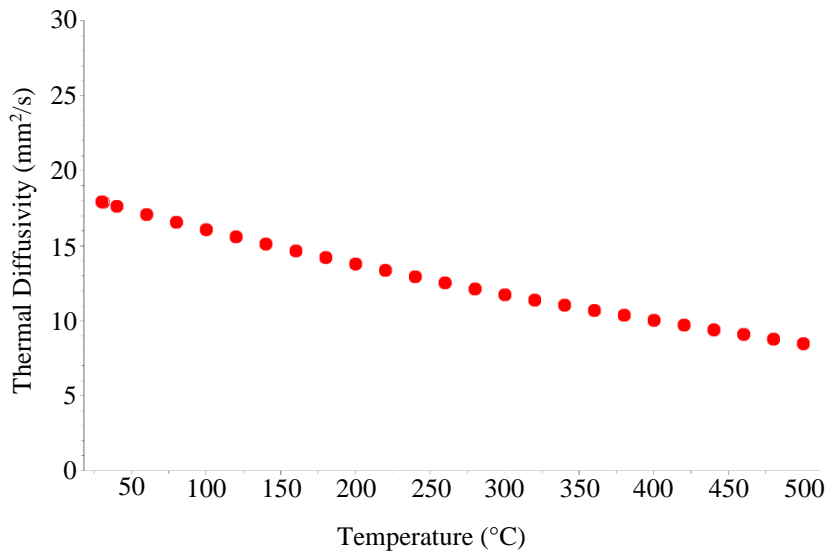
(a) Thermal Diffusivity Measurements
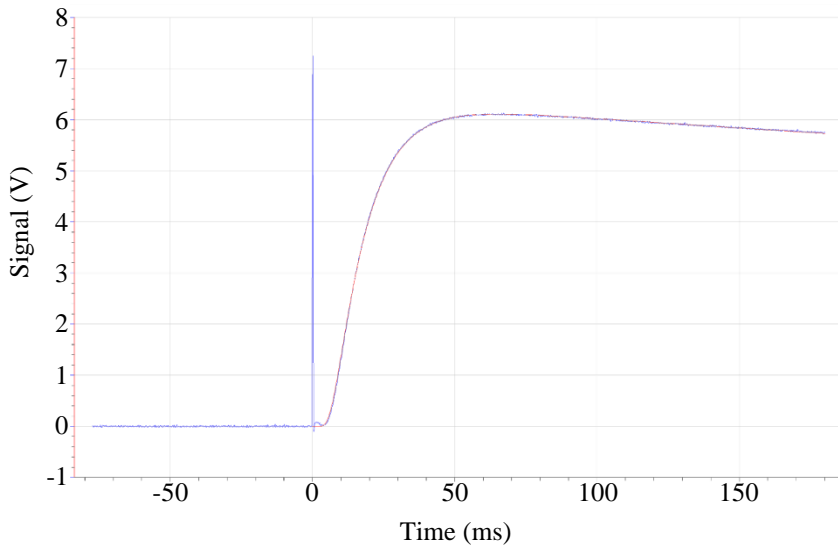
(b) Measured Temperature versus Time Curve at 300°C

Figure 17: LFA Measurements for Grade 500 Steel
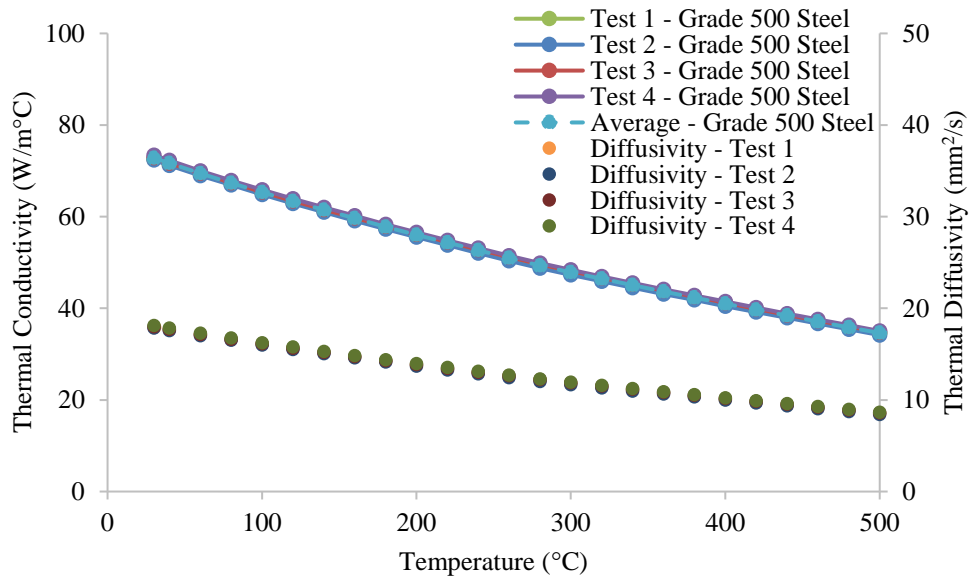
Figure 18: Plots of Thermal Diffusivity and Thermal Conductivity Variations for Grade 500 Steel
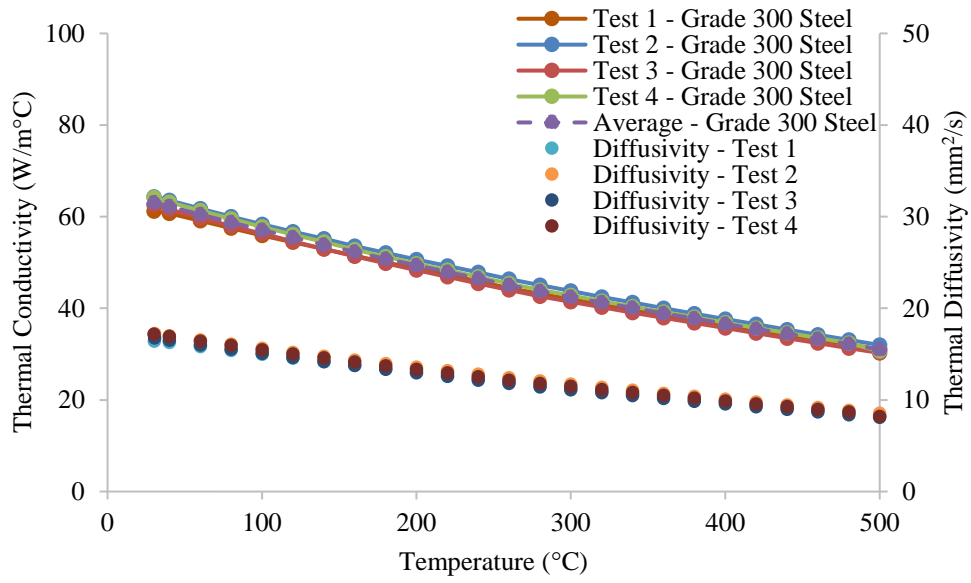
Figure 19: Plots of Thermal Diffusivity and Thermal Conductivity Variations for Grade 300 Steel
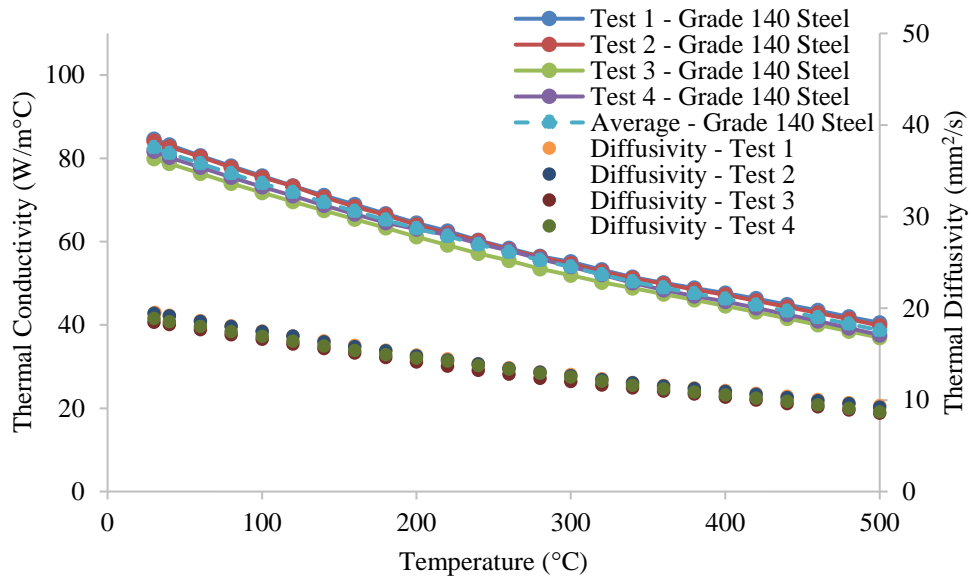
Figure 20: Plots of Thermal Diffusivity and Thermal Conductivity Variations for Grade 140 Steel
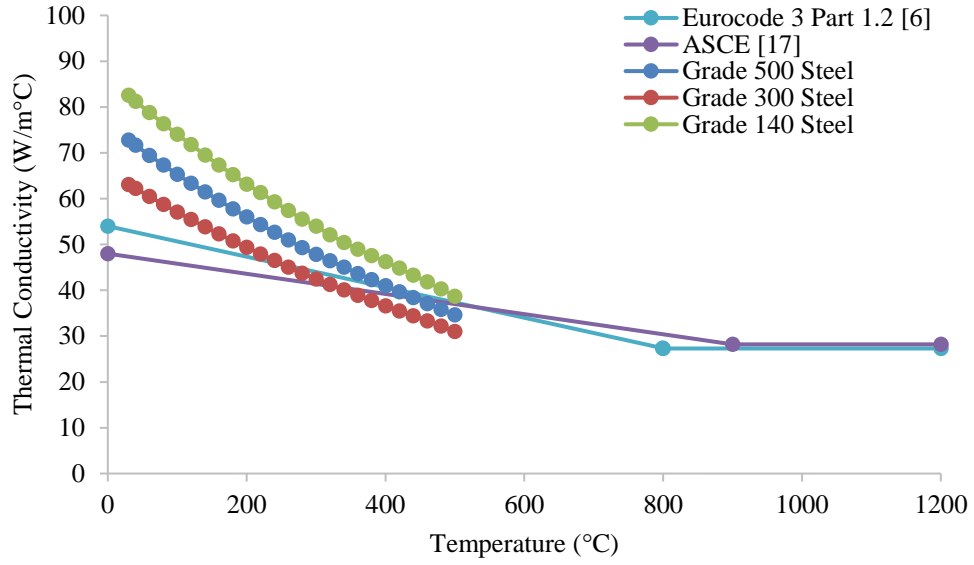
Figure 21: Comparison of Thermal Conductivity Values of Cold-Formed Carbon Steels with Eurocode 3 Part 1.2 and ASCE Models
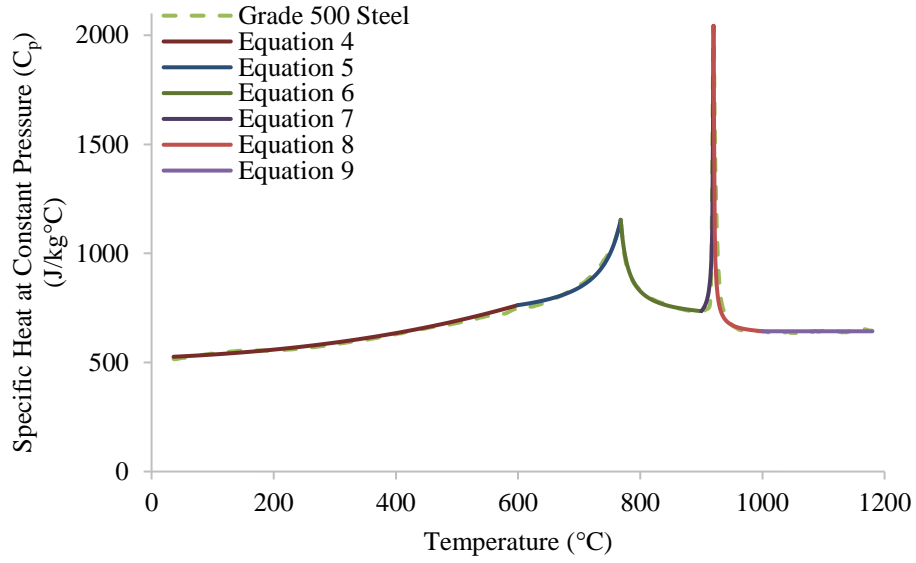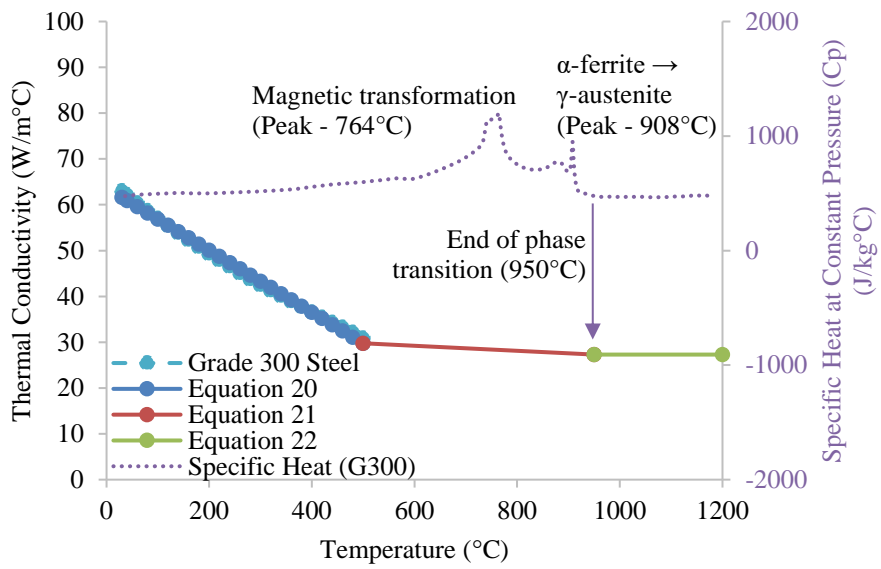
(a) Specific Heat at Constant Pressure
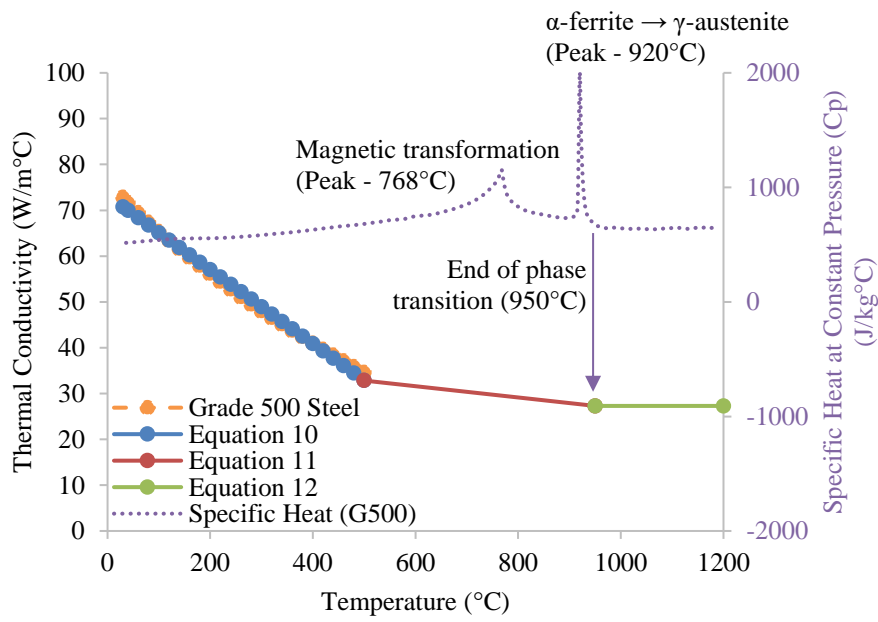
(b) Thermal Conductivity

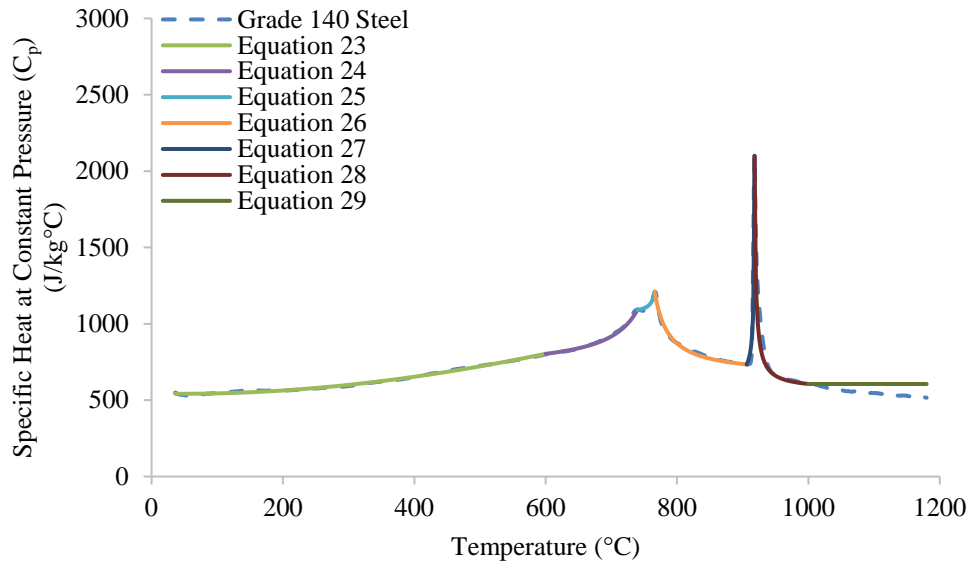**Figure 22: Proposed Equations for Grade 500 Steel**
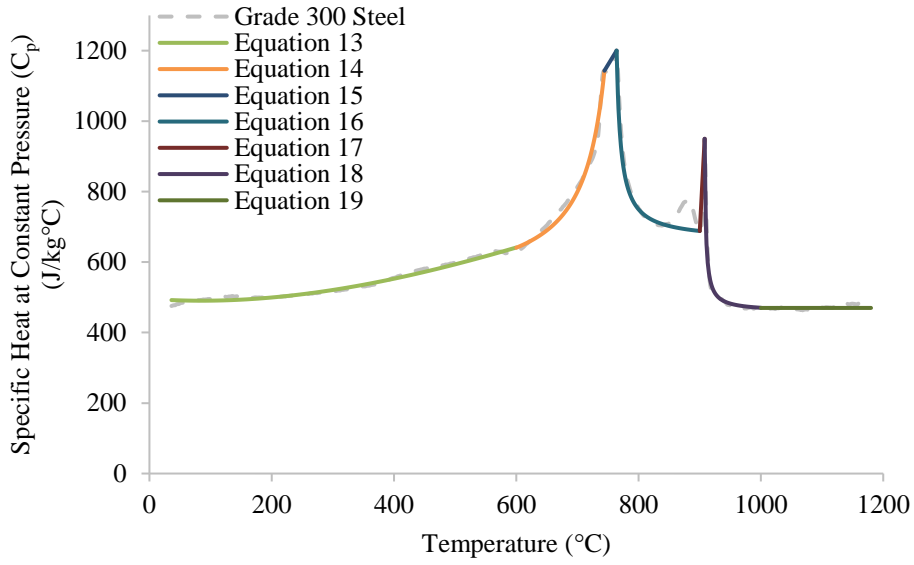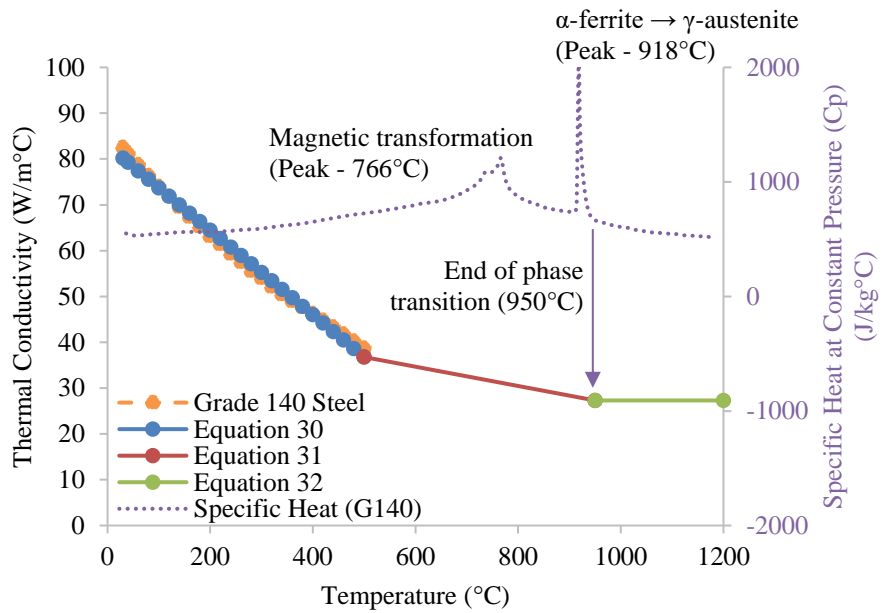
(a) Specific Heat at Constant Pressure

(b) Thermal Conductivity

Figure 23: Proposed Equations for Grade 300 Steel

(a) Specific Heat at Constant Pressure

(b) Thermal Conductivity

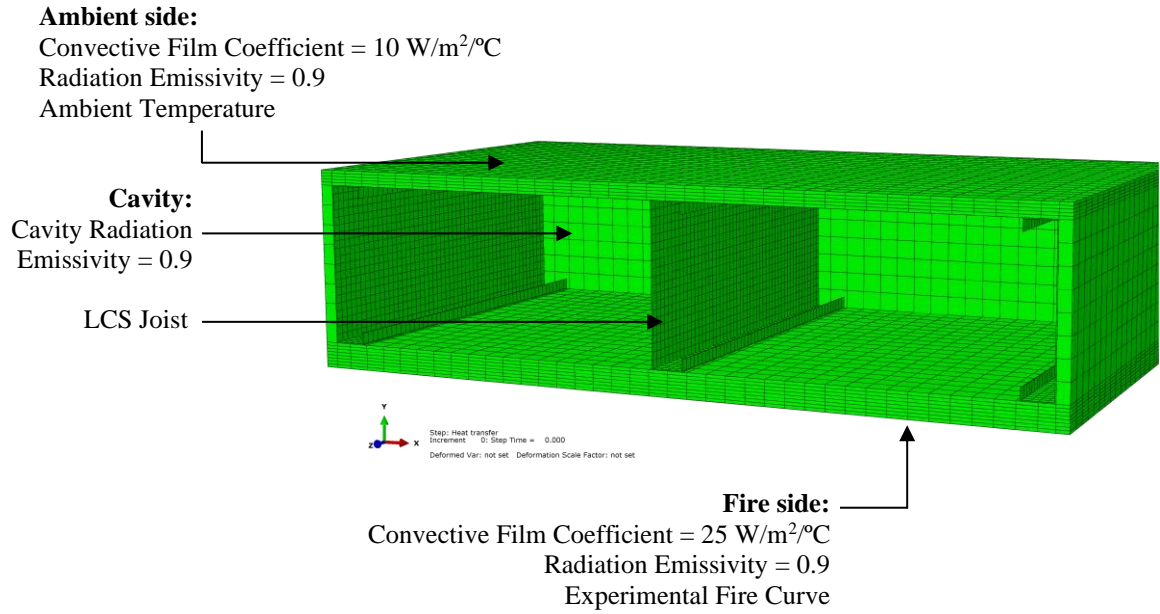**Figure 24: Proposed Equations for Grade 140 Steel**

Ambient side:
Convective Film Coefficient = 10 W/m^2/°C
Radiation Emissivity = 0.9
Ambient Temperature

Cavity:
Cavity Radiation
Emissivity = 0.9

LCS Joist

Step: Heat transfer
Increment   0: Step Time =   0.000
Deformed Var: not set   Deformation Scale Factor: not set

Fire side:
Convective Film Coefficient = 25 W/m^2/°C
Radiation Emissivity = 0.9
Experimental Fire Curve

Figure 25: Finite Element Model of LSF Floor-Ceiling Systems made of LCS Joists

19 mm Plywood

Empty Cavity

LCS Joist
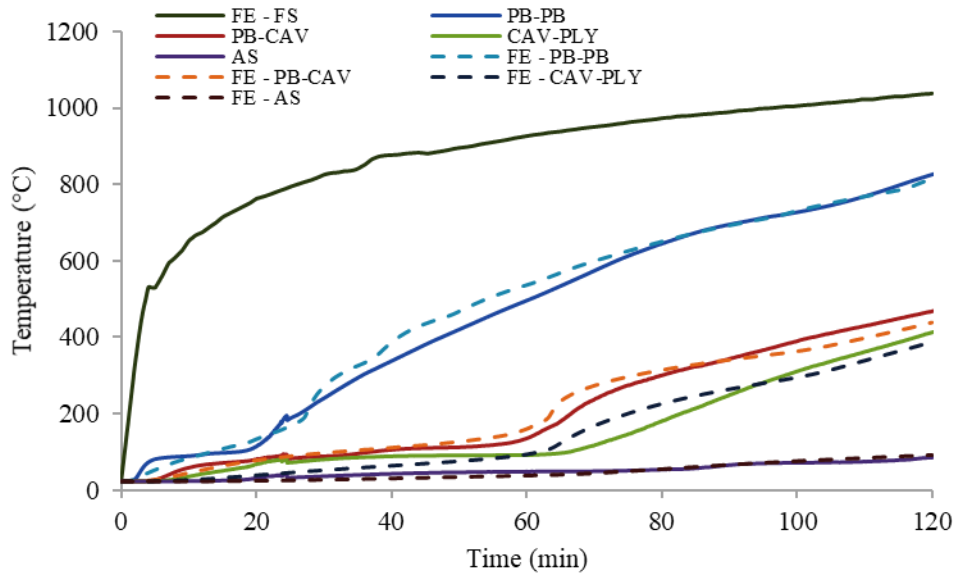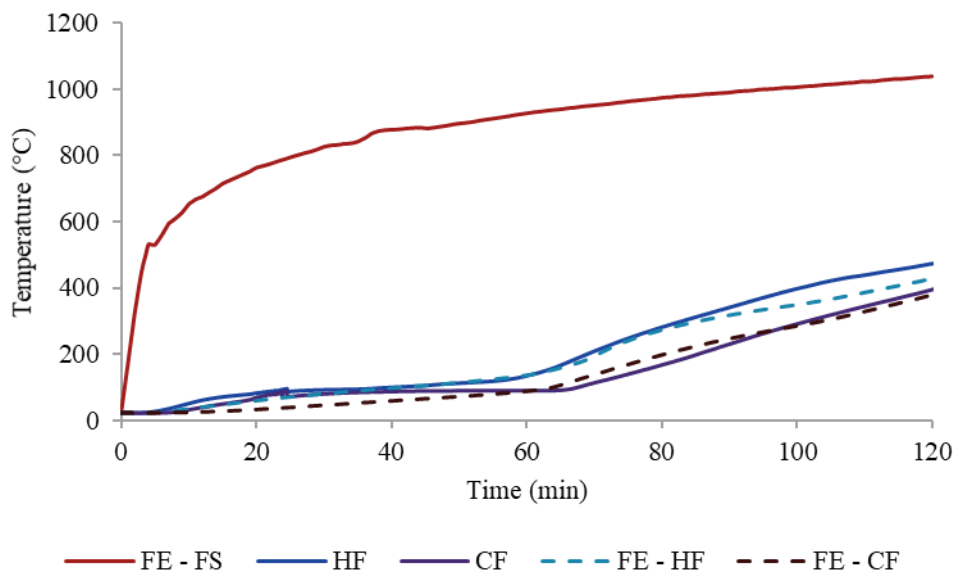
Two Layers of 16 mm Gypsum Plasterboard
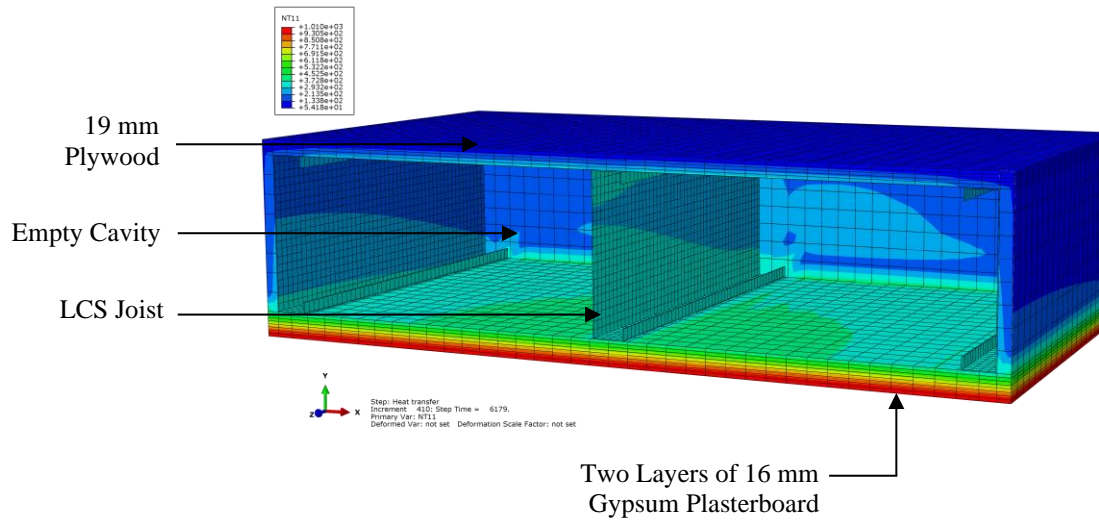
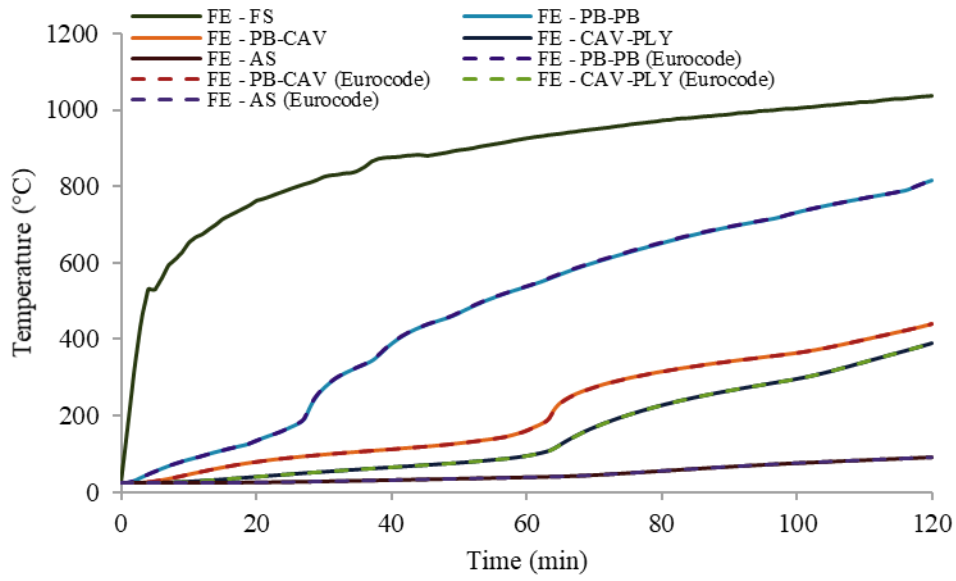**Figure 26: Temperature contours across LSF Floor-Ceiling Systems made of LCS Joists**

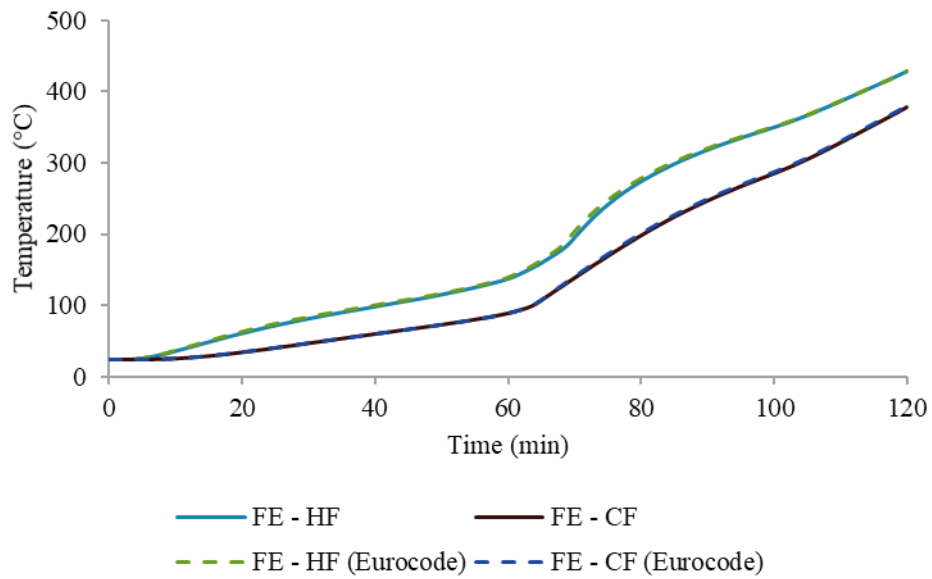(a) Time-temperature profiles at different interfaces across the depth

(b) Time-temperature profiles across LCS joist

Figure 27: Time - Temperature Profiles of LSF Floor-Ceiling Systems made of LCS Joists

(a) Time-temperature profiles at different interfaces across the depth

(b) Time-temperature profiles across LCS joist

Figure 28: Predicted Time - Temperature Profiles based on the Proposed and Eurocode Thermal Property Models